High reactivity of the nickel-rich LiNi1-x-yMnxCoyO2 layered materials surface towards H2O/CO2 atmosphere and LiPF6-based electrolyte

Ana Cristina Martinez, Sylvie Grugeon, Dominique Cailleu, Matthieu Courty, Pierre Tran-Van, Bruno Delobel, Stéphane Laruelle

High reactivity of the nickel-rich $LiNi_{1-x-y}Mn_xCo_yO_2$ layered materials surface towards H_2O/CO_2 atmosphere and $LiPF_6$-based electrolyte

Ana Cristina Martinez[a,b,d], Sylvie Grugeon[a,b], Dominique Cailleu[c], Matthieu Courty[a,b],

Pierre Tran-Van[d], Bruno Delobel[d], Stephane Laruelle[a,b*]

[a]*Laboratoire de Réactivité et Chimie des Solides, CNRS UMR 7314, Université de Picardie Jules Verne, 33 rue Saint Leu, 80039 Amiens, France*
[b]*Réseau sur le Stockage Electrochimique de l'Energie, CNRS RS2E FR3459, France*
[c]*Plate-Forme Analytique, Université de Picardie Jules Verne, 33 rue Saint Leu, 80039 Amiens, France*
[d]*Renault, DEA-IREB, Technocentre, 1 avenue du Golf, 78288 Guyancourt, France*

[*]*corresponding author: stephane.laruelle@u-picardie.fr*
Tel: +33 322825778

Abstract:

Storage of nickel-rich $LiNi_{1-x-y}Mn_xCo_yO_2$ positive active materials under improper environmental conditions brings about undesirable surface reactions causing poor Li-ion cell electrochemical performances and gas generation. In this paper, a detailed stepwise investigation of the increasing reactivity of 532, 622, 811 and 901 NMC materials towards a specific H_2O/CO_2 atmosphere is reported. Water-soluble salts as lithium carbonate, hydroxide and sulfates are accurately quantified thanks to acid-base titration and inductively coupled plasma atomic emission spectroscopy techniques. On the other hand, the presence of insoluble species as transition metal oxyhydroxides and oxides is unveiled through a thermal decomposition study using thermogravimetric mass spectrometer coupling technique. Their formation and thermal decomposition mechanisms are proposed after careful analysis of the characteristic mass loss and O_2, CO_2 and H_2O evolution profile in the 50-500°C region. Interestingly, the results also highlight an *in situ* lithiated layered oxide material reformation reaction. To assess their chemical reactivity towards $LiPF_6$-based electrolyte, the latter was analyzed through ^{19}F nuclear magnetic resonance after storage with various reference salts and 811 NMC. $LiPO_2F_2$ is detected from storage tests with

Li_2CO_3, Li_2O and Li_2SO_4, and fluorophosphate-type molecules are detected from LiOH; this experiment can help discriminate between LiOH and Li_2O as NMC surface species.

Keywords: NMC storage, titration, TG-MS, $LiPO_2F_2$, soluble base

1. Introduction

Surface layers of layered positive electrode materials such as nickel, manganese and cobalt-based $LiNi_{1-x-y}Mn_xCo_yO_2$ play an important role on capacity retention upon cycling [1–6] as well as on electrode laminate processing steps during battery production [7,8]. Over the last decade, these materials have been entering the electric vehicle lithium-ion batteries (LIBs) composition, therefore extensive studies aimed at identifying the surface species composition and understanding their formation mechanism have been undertaken. Nickel-rich NMC materials ($x > 0.5$) have been particularly investigated as they offer higher energy density, but, unfortunately are also prone to higher instability towards air environment [5,9,10].

Li_2CO_3 and LiOH were the most widely reported surface species in the literature [2–4,7,8,10–18]. Fourier transform infrared spectroscopy (FTIR) [11] and X-ray photoelectron spectroscopy (XPS) [13] helped identify Li_2CO_3. Furthermore, X-ray diffraction (XRD) [4,14,19], ionic chromatography [16] and gas chromatography [10] turned out to be powerful techniques to quantify it whereas titration technique was mostly used to quantify both Li_2CO_3 and LiOH [2,3,7,8,17,18]. These compounds, commonly referred to as soluble bases (SB) are either residual from the layered material synthesis or developed upon storage in ambient atmosphere.

Most of the time, their formation is associated with the presence of a rocksalt-type NiO or $Li_xNi_{1-x}O$ phase [14,20]. As depicted from XPS analysis, these phases entail a redox process, *i.e.* the reduction of trivalent to divalent nickel. This reaction would concomitantly produce active oxygen species alongside with soluble bases as follows [11,20] [Eqs 1-4] :

$$Ni^{3+} + O^{2-}_{(lattice)} \rightarrow Ni^{2+} + O^{-} \quad [1]$$

$$O^{-} + O^{-} \rightarrow O^{2-}_{(active)} + O \quad [2]$$

$$O^{2-}_{(active)} + CO_2 \rightarrow CO_3^{2-} \quad [3]$$

$$O^{2-}_{(active)} + H_2O \rightarrow 2OH^{-} \quad [4]$$

Another mechanism was established from XRD results. The substitution of NMC lithium cations by protons is assumed to explain structural changes, which would not imply any redox reaction; soluble bases would result from the reaction of lithium cations with H_2O and/or CO_2 [13].

Some studies also supposed, without actual evidence, the presence of lithium bicarbonate, $LiHCO_3$, [5,20]. However, this hypothesis should be discarded for the reason that, according to thermodynamic data on $LiHCO_3$, this compound is only stable in solution [21]. Recently, some authors also proposed the formation of $NiCO_2.2Ni(OH)_2.xH_2O$ (zaratite) from RAMAN spectroscopy and thermogravimetric/mass spectrometry (TG-MS) measurements [10,22]. It is worth noting that, unlike the above-mentioned compounds Li_2CO_3, LiOH and $LiHCO_3$, this nickel hydroxycarbonate is insoluble in water [23].

Overall, these studies reveal that determining the exact surface impurity species composition at the extreme surface of NMC materials is still challenging, which is understandable when considering the very thin developed layer (5-20nm [24]). As there is no general agreement regarding the soluble bases global formation mechanism occurring upon air environment storage, we settled on undertaking a quantitative study on different NMC

materials exposed or not to H_2O/CO_2 environment, by making use of complementary acid-base titration (ABT) and inductively coupled plasma atomic emission spectroscopy (ICP-AES) techniques. Additional TG-MS measurements were performed on these materials, thus enabling to highlight a novel formation mechanism.

Besides, in an attempt to understand further the role of these surface species upon cycling, we focused on their chemical fate while in contact with the $LiPF_6$-based electrolyte. Some studies have indeed exhibited an actual reactivity of Li_2CO_3 with electrolyte, producing P-F containing species precipitated at the surface of NMC particles [25,26]. On the basis of these results, we started an analytical study by means of ^{19}F nuclear magnetic resonance spectroscopy (NMR), to get a comprehensive insight into the reactivity of the identified species, as reference pure compound, and then, as part of the NMC surface layer, upon storage at 20 and 55°C in electrolyte.

2. Experimental

2.1. Layered materials

$LiNi_{0.5}Mn_{0.3}Co_{0.2}O_2$ (532), $LiNi_{0.6}Mn_{0.2}Co_{0.2}O_2$ (622), $LiNi_{0.8}Mn_{0.1}Co_{0.1}O_2$ (811), $LiNi_{0.9}Co_{0.1}O_2$ (901), and alumina-coated $LiNi_{0.6}Mn_{0.2}Co_{0.2}O_2$ (622C) were supplied by Umicore (BET surface area ≈ 0.25 m^2g^{-1}, particle size D50 ≈ 11.7µm). All powders were weighed and handled in an argon-filled glove box (< 0.1 ppm O_2 and H_2O, MBraun) to avoid air exposure.

2.2. Materials exposed to H_2O/CO_2 atmosphere

12 g of NMC materials were stored in a desiccator during 6 days in a controlled atmosphere of 8/92 (molar ratio) CO_2/Ar mixture with a 90% RH at 35°C. After exposure, the samples were vacuum-dried in a glass oven (Büchi, Switzerland) for 24h at 110°C prior to being transferred to the argon-filled glove box.

2.3. Characterization of surface species

Scanning electron microscopy images of selected samples were carried out by means of a field emission gun scanning electron microscope fitted with an energy dispersive X-ray spectrometer (SEM-EDX, Oxford Instrument), operating at 15 kV. The exposed materials were covered with a conductive gold layer before the analysis.

2.4. Quantification of surface species

5 g of NMC material were magnetically stirred in 100 g of bi-distilled water, for 8 or 10 minutes, depending on the nickel content (see Results and discussion section). Thereafter, the powder was recovered through vacuum filtering. Half of the filtrate solution was titrated to quantify the basic species by means of an automatic titrimeter equipped with pH electrode (TitroLine 7000, SI Analytics GmbH). The solution was magnetic stirred under argon bubbling in an adapted closed flask fitted and titrated by a solution of HCl 0.05 M. ICP-AES (Varian 720 ES) analysis was carried out on the remaining half of the solution. Every analysis was performed at least three times to ensure reproducibility.

2.5. Thermogravimetric analysis coupled with mass spectrometry (TG-MS)

The as-received and exposed to H_2O/CO_2 atmosphere NMC materials were analyzed by TG-MS using a STA 449F3 (NETZSCH, Germany) instrument located in a argon-filled glove box (< 0.1 ppm O_2 and H_2O, Jacomex). The TG-MS experiments were performed from 25 to 900°C at a rate of 5 K min^{-1} under argon atmosphere at a flow rate of 40 mL min^{-1}.

2.6. Chemical reactivity with electrolyte

The reference materials Li_2CO_3 (> 99%) and Li_2O (97%) were purchased from Sigma-Aldrich. Li_2SO_4 was obtained by vacuum-drying at 130°C of $Li_2SO_4.1H_2O$ (Sigma-Aldrich, 99%). LiOH was synthesized by Li reaction with methanol then vacuum-dried. The reference material

(with a reference material-to-$LiPF_6$ molar ratio of 1.35) or 100 mg of NMC material was added to 1mL of an electrolyte solution consisting in 1M $LiPF_6$ in a 1:1:1 vol. mixture of EC/DEC/EMC (99.9%, H_2O < 20 ppm - Solvionic). The mixtures were put into an aluminum laminated film for pouch cell for four days of storage at 25 or 55°C. The chemical inertness of the bag towards the electrolyte was verified prior the experiments. After storage, 0.5 mL of the electrolyte was recovered in the glove box by centrifugation and transferred to an NMR tube for liquid ^{19}F NMR analysis (Bruker Ultrashield 400 MHz). The fluorine (376.5 MHz) spectra were acquired with a 5-mm nitrogen cryoprobe and recorded with a relaxation delay of 5 s prior to one 90 ° pulse excitation (13.5 µs) and an acquisition time of 0.8 s (total relaxation for relative quantification).

3. Results and discussion

3.1. Surface species analysis

3.1.1. Washing procedure optimization for acid-base titration and ICP-AES analyses

The amount of hydroxides and carbonates issuing from the surface of the NMC powders was determined using the Warder's titration method [27,28]. To do so, these compounds were solubilized in an aqueous solution containing a 1:20 NMC powder-to-water weight ratio and the whole system was kept under argon bubbling to avoid the acidification of the solution with CO_2 in air.

Due to the increased reactivity of high-Ni layered materials [29], the stirring time of the NMC containing aqueous solution was adapted as function of the nickel composition. For that purpose, the pH variation was recorded immediately after the introduction of NMC powder in water. Fig. 1a shows the pH variation as function of time for 532, 622C, 811 and 901. The pH increases rapidly up to values of 11.2, 11.8, 12.15 and 12.20 for 532, 622C, 811 and 901,

respectively, which indicates a fast soluble bases dissolution and different concentrations on each NMC surface. Subsequently, the pH tends to stabilize between 5 and 15 minutes of agitation, depending on the nickel composition. From there, the slow but constant pH increase can be explained by the proton exchange phenomenon, that takes place when a lithium ion in the material is substituted by a proton in solution [18,30]. These observations expressed the need to reach a compromise on the stirring time enabling a complete soluble bases solubilization while avoiding, as much as possible, the proton exchange phenomenon. In order to define the agitation time required for each material, the solution was filtrated and titrated after 5, 10, 15 and 30 minutes of stirring time, denoted by the dotted lines in Fig. 1a. The individual acid-base titration results are depicted in Fig. 1b-e.

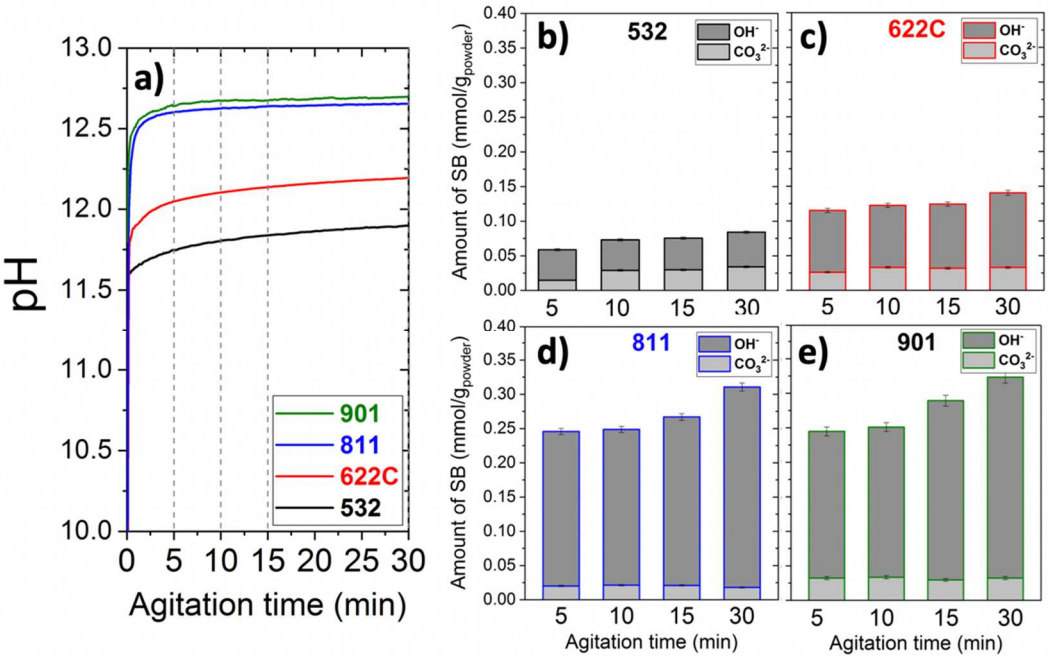

Figure 1: a) Variation of pH values over time for a suspension of 5 g in 100 mL of bi-distilled water for 532, 622C, 811 and 901 materials; the vertical dotted lines in denote the times at which the solution was analyzed by ABT. Amounts of OH^- and CO_3^{2-} determined by ABT of the filtrate solution at different agitation times for b) 532, c) 622C, d) 811 and e) 901.

The CO_3^{2-} concentration reaches a maximum value at 10 minutes for 532 and 622C and at 5 minutes of stirring time for 811 and 901 NMC materials. As for OH^- concentration, it remains constant around 10 to 15 minutes for 532 and 622C and 5 to 10 minutes of stirring time for 811 and 901; it increases right after, as a result of the proton exchange dominating process that arises during long water exposures. Considering these variations, the agitation time was fixed at 15 minutes for 532, 622 and 622C, and 8 minutes for 811 and 901.

3.1.2. Quantification of OH^- and CO_3^{2-} by acid-base titration

The amounts of CO_3^{2-} and OH^- obtained by acid-base titration from each as-received NMC material are shown in Table 1. The OH^-concentration varies between 0.040 and 0.214 mmol/ $g_{\text{active material powder (AM powder)}}$, increasing with the nickel content from 532 to 901. The CO_3^{2-} quantity does not vary as much and reaches a maximal value of 0.040 mmol/$g_{\text{AM powder}}$ in every material. It is worth noting that there is no significant difference between the coated and uncoated 622 material, unveiling that this type of alumina coating does not interfere with soluble bases dissolution, most probably because the particles surface is unevenly covered, as shown by SEM (Fig. S1).

mmol/$g_{\text{AM powder}}$	**532**	**622C**	**622**	**811**	**901**
OH^-	0.040 ± 0.001	0.090 ± 0.002	0.103 ± 0.003	0.214 ± 0.005	0.214 ± 0.005
CO_3^{2-}	0.018 ± 0.001	0.037 ± 0.002	0.040 ± 0.002	0.019 ± 0.001	0.039 ± 0.002

Table 1**:** Amounts of OH^- and CO_3^{2-} determined by ABT after 15 minutes of washing time for 532, 622, 622C, and 8 minutes for 811 and 901.

Interestingly, all NMC materials FTIR spectra (Fig. S2) revealed bands at 878, 1425 and 1500 cm^{-1} assigned to CO_3^{2-} species. However, the characteristic band of LiOH near 3675 cm^{-1} is

absent, which raises questions about its presence. This point will be further discussed in section 3.3.2.

3.1.3. Quantification of lithium, sodium and sulfur by ICP-AES

Acid-base titration technique has proven to be a powerful technique for the accurate quantification of OH^- and CO_3^{2-} basic species, however, ICP-AES analysis of the washing solutions was required as a complementary technique to unveil the presence of other possible soluble salts.

Lithium, sodium and sulfur elements are detected in noticeable concentrations. The presence of sodium and sulfur elements does not come as a surprise as MSO_4 (M= Ni, Mn and Co) and NaOH are used as reagents in the NMC materials industrial synthesis process [18]. The presence of sulfate species was also confirmed by FTIR (Fig. S2); each NMC spectrum reveals bands at around 1125 cm^{-1} that can be assigned to SO_4^{2-}. Several particles containing both sodium and sulfur elements, ascribed to Na_2SO_4, were also found by SEM/EDX (Fig. S3).

For the sake of comparison, Fig. 2 shows both ICP-AES and acid-base titration results. Assuming that all OH^- and CO_3^{2-} detected by ABT were lithium salts, their concentrations were converted into lithium concentrations with the respective molar equivalences of 2 and 1 for Li_2CO_3 and LiOH.

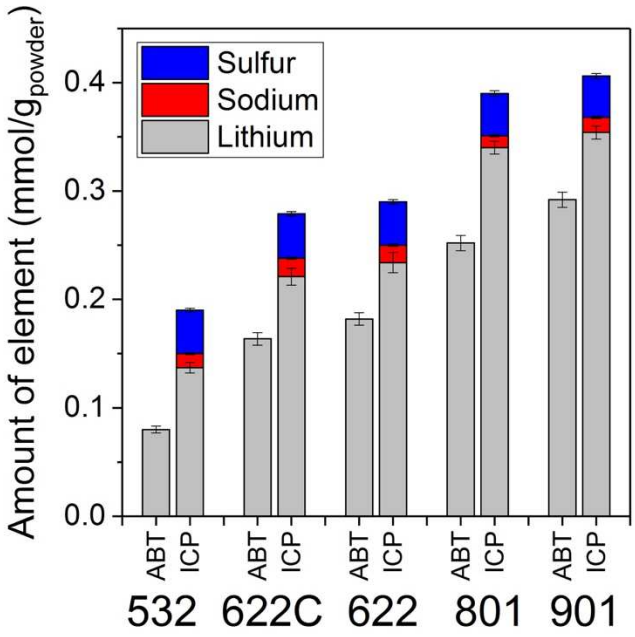

Figure 2: ABT and ICP-AES results comparison of lithium, sodium and sulfur elements in the filtrate solutions. Assuming that all soluble bases detected by ATB were lithium salts, their concentrations were converted into lithium concentrations with the respective molar equivalences of 2 and 1 for Li_2CO_3 and LiOH.

Results from both techniques show an increase of total lithium amount with increasing Ni amount in NMC materials as also reported by Noh *et al.* [29]. Lithium concentration values detected by ICP-AES are found to be higher for each material. This leads to the conclusion that some soluble lithium salts are not titrated due to a weak base characteristic or a non acid-base property. Sodium and sulfur were detected in all samples and their concentrations equal to 0.014 ± 0.003 and 0.040 ± 0.002 mmol/$g_{AM\ powder}$, respectively. Assuming that the sulfur element detected by ICP-AES originates from sulfate(s) and considering the additional lithium, sodium and sulfur concentrations detected by ICP-AES, it can be inferred that these elements are stemming from Li_2SO_4 and Na_2SO_4 compounds.

The complementarity of the two techniques allowed the identification of all soluble bases in the five types of NMC material and gave reliable quantification results. Furthermore, evidence was given that, contrary to the common knowledge, Li_2CO_3 and LiOH are not the only soluble species in as-received materials, there are also sulfate species. Those sulfates M_2SO_4 (M = Li, Na) are present in all samples with an equal concentration of 40 µmol/$g_{AM\ powder}$. On the other hand, Li_2CO_3 and LiOH concentration values increase from 18 to 40 and from 40 to 214 µmol/$g_{AM\ powder}$, respectively, with the nickel content in the different NMC materials.

3.2. Influence of H_2O/CO_2 exposure

Since the early 2000's, several investigations have been devoted to defining the impact of air exposure [4,5,8–10,12–14,16,19,20,22,31,32] on NMC particles. However, despite these very interesting works, reaction mechanism(s) regarding surface species formation still lack of clarification, which incited us to further investigate and expand the study to the comparative reactivity of the different NMC compositions towards a similar H_2O/CO_2 exposure. The study of the surface species composition has been carried out by making use of acid-base titration and TG-MS techniques with a view to gain insight into the reaction mechanism involved.

3.2.1. Quantification of OH^- and CO_3^{2-} by acid-base titration

The amounts of soluble bases detected by acid-base titration in the as-received and the exposed NMC materials are displayed in Figs 3 a and b. The materials surface composition is quite different as hydroxide anion is mostly detected in the as-received materials, while carbonate anion is the main species detected after H_2O/CO_2 exposure. The same trend was already observed in literature with 532 material (D50 ≈ 12 µm) exposed for one year in air, with LiOH values of 23 and 15 µmol/$g_{AM\ powder}$ and Li_2CO_3 values of 15 and 38 µmol/$g_{AM\ powder}$

before and after exposure, respectively [8]. These results indicate the transformation upon exposure of the LiOH contained in pristine materials into Li_2CO_3. As demonstrated by William *et al.* [33], the reaction takes place following a two-step process with hydrated lithium hydroxide as intermediary species [Eqs 5 and 6]:

$$2LiOH + 2H_2O \leftrightarrow 2LiOH.H_2O \quad [5]$$

$$2LiOH.H_2O + CO_2 \rightarrow Li_2CO_3 + 3H_2O \quad [6]$$

After exposure, LiOH is detected only in the case of the highest Ni content containing NMC materials, 811 and 901, and its concentration does not exceed 50 µmol/$g_{AM\ powder}$. It is worth noting that the 811 values are close to the ones reported in literature for a 811 material (diameter of c.a. 25µm) exposed for 7 days in air, as being 82 and 257 µmol/$g_{AM\ powder}$ for LiOH and Li_2CO_3, respectively [34]. The most significant result is the increase of the total soluble bases content in all NMC materials. Their formation requires lithium ions, which implies a delithiation of the material. When becoming prominent, this process induces a surface textural modification clearly observed in SEM images, as exemplified in Fig. 3c and 3d, with the Li_2CO_3 flakes growth at the outermost surface of the exposed 901 material.

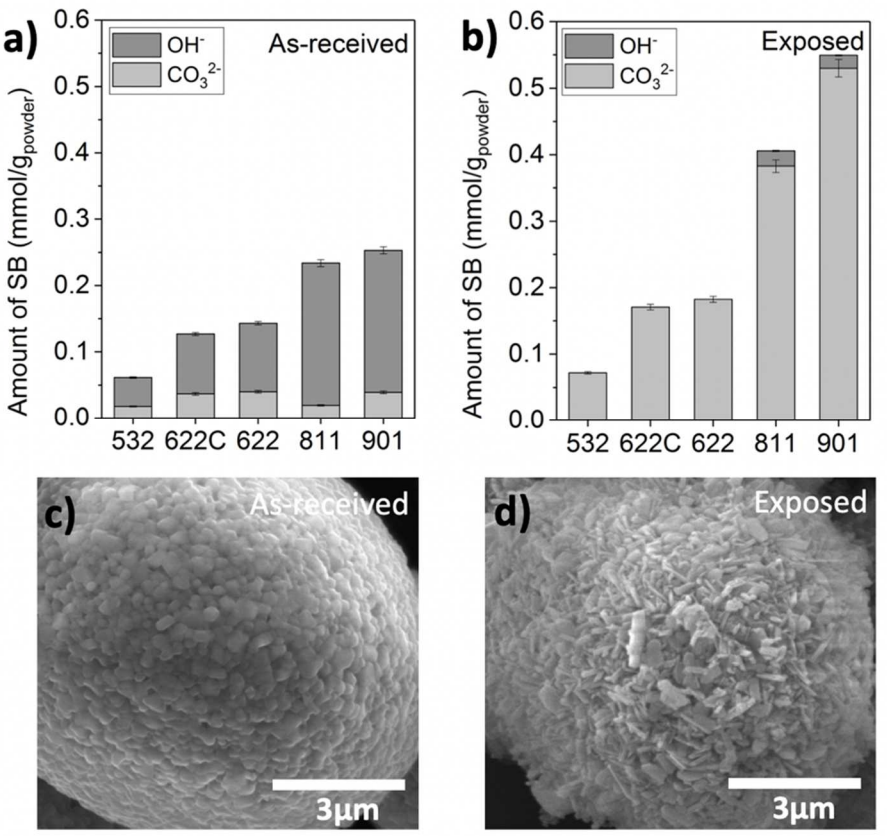

Figure 3: Amounts of OH^- and CO_3^{2-} determined by ABT analysis in the filtrate solution for a) the as-received and b) exposed materials. SEM images of an (b) as-received and (c) H_2O/CO_2 exposed 901 particles.

The extracted lithium quantity was calculated from acid-base titration results (Table 2) assuming, as above-reported, that all detected hydroxide and carbonate were lithium salts. It increases with the amount of nickel in NMC. For the exposed 532, 622 and 622C materials, the molar percentage of extracted lithium does not exceed 2%. Similarly to the above observations on as-received materials, exposed coated and non-coated 622 materials display similar values of 1.72 and 1.77%, demonstrating the inefficiency of the present coating to prevent a surface structure modification upon this specific H_2O/CO_2 exposure. More significantly, values as high as 5 and 8% were reached for 811 and 901 materials,

respectively, in only six days of exposure. For the sake of comparison, Bichon *et al.* [8] reported from titration analysis, an extracted lithium quantity value of 0.3% for a 532 material exposed in air for one year and Matsumoto *et al.* [19], from Li_2CO_3 quantification by XRD, a value of 8% for a NCA material exposed for 500 hours in air. The highest values depicted in case of Ni-rich materials were expected as a higher reactivity towards CO_2 was already reported in literature [35] to depend on Ni^{3+} content in NMC materials, causing severe capacity fade.

Lithium amount	532	622C	622	811	901
as-received ($mmol/g_{AM\ powder}$)	0.080 ± 0.003	0.164 ± 0.006	0.182 ± 0.006	0.252 ± 0.007	0.292 ± 0.007
exposed ($mmol/g_{AM\ powder}$)	0.143 ± 0.004	0.341 ± 0.008	0.365 ± 0.009	0.788 ± 0.020	1.079 ± 0.027
extracted (mol %)	0.63 ± 0.01	1.72 ± 0.01	1.77 ± 0.02	5.30 ± 0.03	7.90 ± 0.03

Table 2: Calculated lithium amount from ABT results for the as-received and exposed materials and calculated lithium molar percentage extracted upon H_2O/CO_2 exposition.

As far as lithium and sodium sulfates quantified in as-received materials are concerned, a question may arise on their chemical behavior when stored in a CO_2/H_2O atmosphere. They are chemically inert to CO_2 gas but would form hydrated sulfates such as $Li_2SO_4.1H_2O$ and $Na_2SO_4.10H_2O$. Based on our ICP-AES results, a maximum H_2O concentration of 150 $\mu mol/g_{AM\ powder}$ could be uptaken. However, sodium sulfate decahydrate is known to decompose peritectically upon heating at 32.4°C to yield anhydrous sodium sulfate along with a saturated aqueous solution of Na_2SO_4 [36] and lithium sulfate monohydrate was found to dehydrate around 100-120°C [37]. Hence, the water removal is expected to occur upon electrodes drying process before cells assembling.

Overall, quantifying soluble bases after exposure in H_2O/CO_2 atmosphere helped estimate the incremental reactivity of NMC materials as function of the nickel content. Such exposure brings about the transformation of LiOH into Li_2CO_3 along with a material delithiation process. For a better understanding of the change in material surface composition, further experiments were conducted using TG-MS techniques.

3.2.2. TG-MS analysis

Thermogravimetric analysis (TGA) was already used [9,20,30,34] as an attempt to capture the composition of surface impurity species grown at the surface of NMC materials upon storage in air. All studies showed, after storage, weight losses in the 35-800°C temperature range. More specifically, three main regions were clearly distinguished. Thanks to complementary TPD-MS analysis on $LiNi_{0.8}Co_{0.2}O_2$, Liu *et al.* [20] were the first to attribute these weight losses, thanks to O_2, CO_2 and H_2O evolution profiles, to removal of superficial water (<100°C), desorption of bicarbonate ($LiHCO_3$), hydroxyl (LiOH) and carbonate species (200-400°C) and then decomposition of Li_2CO_3 in the 680-780°C region. Very recently, Sicklinger *et al.* [34] suggested, from TG-MS patterns analysis, that basic nickel carbonate $NiCO_3.2Ni(OH)_2.2H_2O$ was arguably the major contaminant upon air exposure of NMC materials. Given the different interpretations of the results, we undertook a stepwise investigation of the thermal decomposition of the as-received and exposed NMC materials by TGA-MS up to 900°C, in the hope to shed some new light on species nature and the associated reaction mechanisms.

3.2.2.1. As-received NMC materials

Figs 4 a and b display the TG and O_2 (m/z 32) MS curves for each as-received material. The five materials present no visible weight loss until the characteristic high temperature range

corresponding to the NMC materials decomposition associated with O_2 evolution. The figures clearly demonstrate the influence of the increasing trivalent nickel content, as 532 and 901 materials start decomposition at 800 and 625°C, respectively. As these experiments are performed under argon flow (O_2 < 2ppm), the oxygen partial pressure is too low to stabilize the +III oxidation state of nickel at these high temperatures, leading to its reduction through the following NMC structural transformation exemplified for 811 materials [Eq. 7]:

$$LiNi_{0.8}Mn_{0.1}Co_{0.1}O_2 \xrightarrow[Ar]{\Delta} 0.3LiNi_{1/3}Mn_{1/3}Co_{1/3}O_2 + 0.7NiO + 0.7/2Li_2O + 0.7/4O_2 \quad [7]$$

Noteworthy that H_2O (m/z 18) and CO_2 (m/z 44) evolution profiles do not depict any noticeable signals around the thermal degradation temperatures of 400 and 700°C for LiOH and Li_2CO_3 respectively, suggesting that soluble bases are in too low concentration to be detected. Furthermore, anhydrous lithium and sodium sulfate species are not expected to decompose in the temperature range up to 900°C.

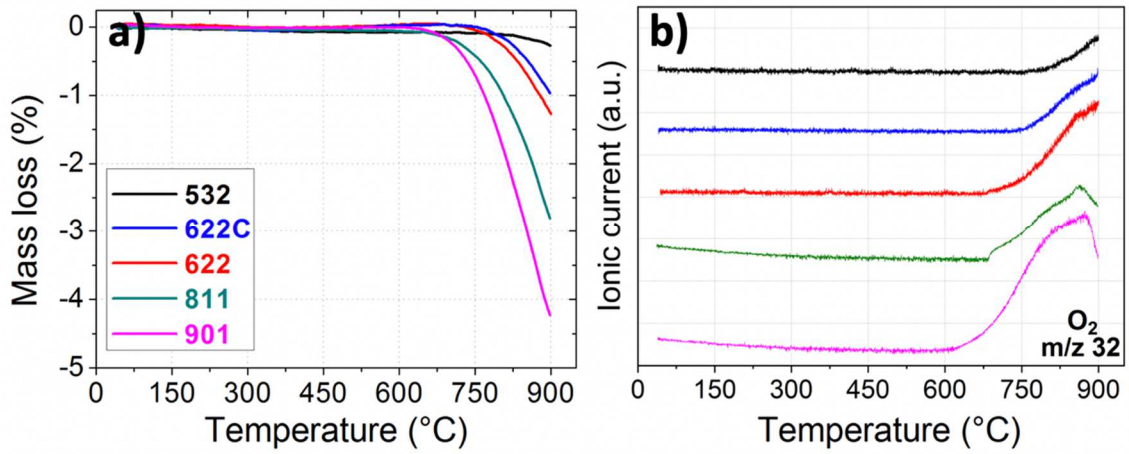

Figure 4: a) TG curves of as-received NMC materials and b) mass traces of O_2 (m/z 32).

3.2.2.2. Exposed NMC materials

According to the above-reported literature on TGA results, the H_2O/CO_2 exposed materials present two main weight loss (Fig. 5a) regions between 150-450°C and above 650°C. The

latter region turns out to be unaffected by the exposure, which is coherent with regard to the material bulk decomposition evolving O_2, as above-mentioned. However, compared to the as-received materials, no additional weight loss peak is observable around 700°C due to Li_2CO_3 decomposition, in spite of its increased concentration with storage as detected by acid-base titration measurements. Only a weak signal in the 700°C region of CO_2 (m/z 44) MS profiles accounts for its presence.

The weight loss in 150-450°C region, pertaining to the decomposition of the surface species formed during the H_2O/CO_2 exposition, increases from 0.4 to 2.13 % with increasing Ni^{3+} amount of NMC materials. Noteworthy that maximum values of 3.7-4 % are reported in literature [9,20].

The gas detected in this region (Figs 5 b-d) are H_2O (m/z 18), CO_2 (m/z 44) and O_2 (m/z 32). First, H_2O evolves from each material between 150 to 300°C, displaying an almost undetectable to a clear two-step signal from 532 to 901 materials. CO_2, on the other hand, is detected between 200-550°C with peak broadening with increasing Ni^{3+} content in NMC. The CO_2 produced at low temperature is highly believed to originate from the decomposition of adsorbed carbonate-containing species. From TPD-MS measurements, comforted by the fact that H_2O and CO_2 peaks evolved at the same temperature of around 270°C, Liu *et al.* [20] proposed the decomposition of the bicarbonate species, $LiHCO_3$, into Li_2O, H_2O and CO_2. However, as discussed in introduction, the existence of $LiHCO_3$ as solid compound can be thermodynamically ruled out. The other reported explanation [34] for H_2O and CO_2 evolution is the decomposition of $MnCO_3.xH_2O$, $CoCO_3.xH_2O$ and an hydroxycarbonate of nickel ($NiCO_3.Ni(OH)_2.xH_2O$). However, from this work, there is no suggested formation mechanism and no clear explanation for the O_2 gas generated around 300°C.

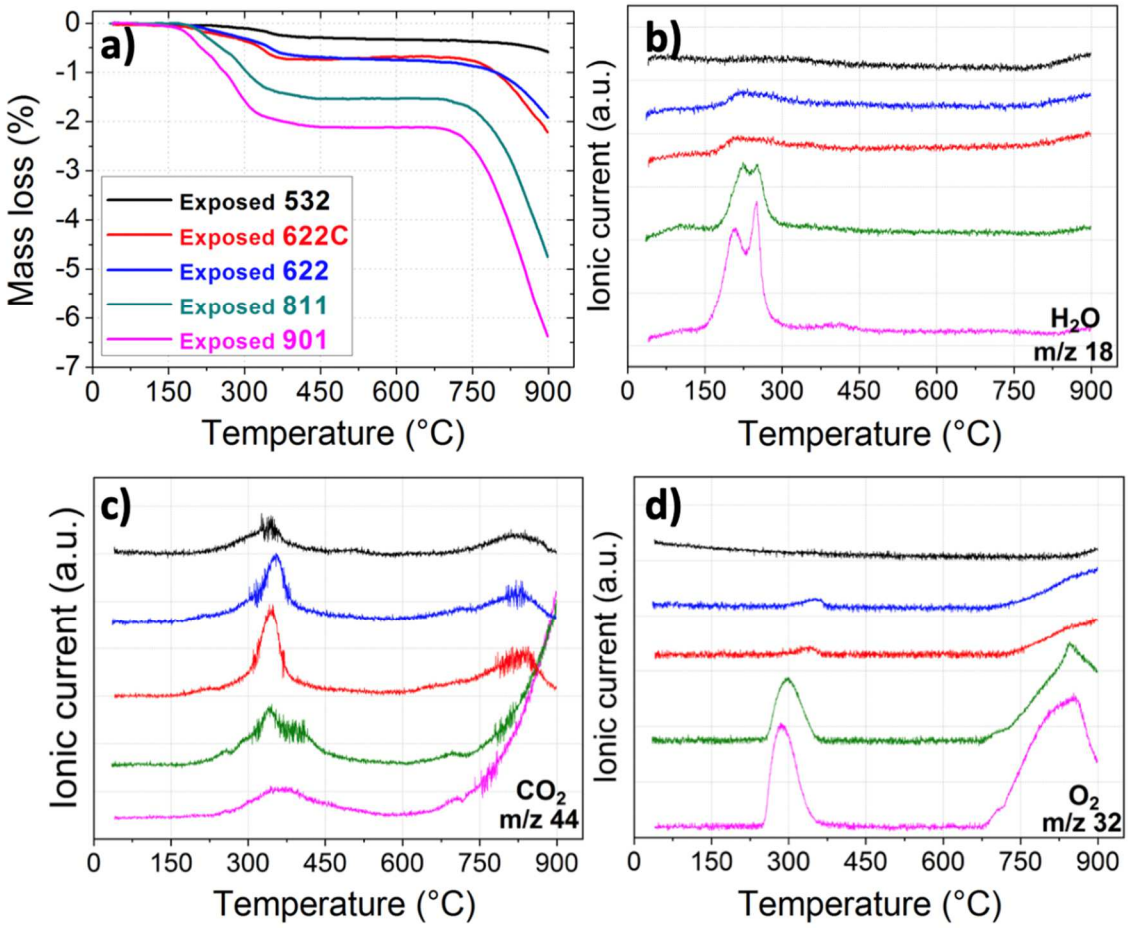

Figure 5: a) TG curves of exposed materials and mass traces of b) H_2O (m/z 18), c) CO_2 (m/z 44) and d) O_2 (m/z 32).

In this work, acid-base titration, ICP-AES and FTIR experiments have provided sound data on the reactivity of NMC materials surface while exposed to H_2O/CO_2 atmosphere. The soluble bases, LiOH and Li_2CO_3 as well as MSO_4 (M=Li and Na), have been identified from the as-received samples washing procedure. Upon exposure, LiOH turns into Li_2CO_3, and further TG-MS experiments proved the occurrence of a surface chemical transformation, increasing with the Ni^{3+} content into the NMC structure. As depicted from acid-base titration analysis, this transformation takes place alongside with Li_2CO_3 growth. Considering that no redox

process takes place during exposure, metallic elements should maintain their oxidation state in accordance with the proposed following reaction [Eq. 8]:

$$LiNi_{1-2x-y}^{(+III)}Ni_x^{(+II)}Mn_x^{(+IV)}Co_y^{(+III)}O_2 \xrightarrow{H_2O/CO_2} 1/2Li_2CO_3 + (Ni_{1-2x-y}Co_y)^{(+III)}OOH + xNi^{(+II)}O + xMn^{(+IV)}O_2 \quad [8]$$

The formation of an oxyhydroxide is supported by the fact that typically, nickel oxyhydroxide is thermally decomposed between 150-400°C to form NiO along with H_2O and O_2 [38–40], according to Eq. 9, precisely the temperature range where O_2 and H_2O are detected in these MS experiments.

$$(Ni_{1-2x-y}Co_y)OOH \xrightarrow{\Delta} (Ni_{1-2x-y}Co_y)O + 1/2H_2O + 1/4O_2 \quad [9]$$

However, the formation of these compounds does not explain the CO_2 production in the 250 -450°C range, as the decomposition of Li_2CO_3 occurs around 700°C. To get more insight into the thermal decomposition processes, an exposed 811 sample was washed with water to eliminate Li_2CO_3 then dried. Afterwards, the sample was analyzed by TG-MS under the same previous conditions.

Fig. 6 shows the comparison of the exposed 811 before and after washing. Up to around 300°C, the weight loss profile is identical for both samples and both H_2O and O_2 gas evolve in a similar way. This result supports the above mechanisms [Eqs 8 and 9] involving the formation of water-insoluble oxyhydroxides that remain at the particles surface after the washing procedure. Beyond this temperature, the weight loss depicted for the washed exposed material is less important (of 0.35 wt. %) than for the exposed sample. The CO_2 gas is almost undetectable along the complete temperature range, indicating that nearly all the Li_2CO_3 was removed from the surface. Considering these results, we propose that the following chemical reaction [Eq. 10] occurs upon the thermal analysis:

$$(Ni_{1-2x-y}Co_y)O + 1/4O_2 + 1/2Li_2CO_3 \xrightarrow{\Delta} Li(Ni_{1-2x-y}Co_y)O_2 + 1/2CO_2 \quad [10]$$

This reaction cannot take place after the washing procedure, as it requires the presence of Li_2CO_3. The oxide-type reactant is formed upon H_2O/CO_2 exposition [Eq. 8] or, *in situ*, along with O_2, from thermal decomposition of nickel oxyhydroxide [Eq. 9]. It is worth noting that this reaction yields lithiated lamellar oxide compound which may explain why, after annealing of air-exposed NMC materials, researchers observe a partial cell capacity retention recovery [41].

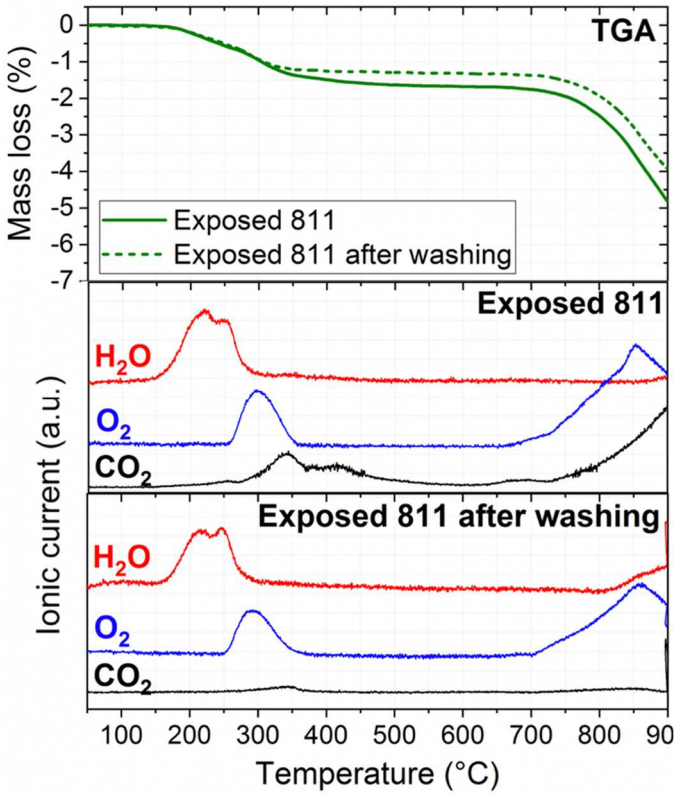

Figure 6: TG curve along with mass traces of H_2O (m/z 18), O_2 (m/z 32) and CO_2 (m/z 44) of an exposed 811 and exposed 811 after washing.

Very recently, Jeong *et al.* [42] and Pritzl *et al.* [30] also proposed the formation of CoOOH and NiOOH compounds at the surface of $LiCoO_2$ and Ni-rich NMCs, respectively, due to Li^+/H^+

exchange upon washing procedure. Interestingly, same O_2 (m/z 32) and H_2O (m/z 18) TG-MS profiles were obtained from their water-washed compounds between 120 and 450°C, without CO_2 (m/z 44) evolution, which supports our hypothesis of *in situ* reaction of Li_2CO_3 consumption [Eq. 10].

Overall, these experiments gave evidence of the chemical reaction of NMC materials under H_2O/CO_2 atmosphere to yield a variety of water-soluble as Li_2CO_3 and LiOH soluble bases, and MSO_4 (M=Li, Na) as well as water-insoluble surface species as rocksalt-type oxide, MnO_2, $(Ni_{1-2x-y}Co_y)O$ and oxyhydroxide $(Ni_{1-2x-y}Co_y)OOH$. These results allowed to propose their formation and thermal decomposition mechanisms through quantitative experiments as titration, ICP-AES and careful analysis of H_2O, CO_2 and O_2 evolution from TG-MS experiments.

3.3. Reactivity of surface species towards electrolyte

With the aim of exploring the chemical reactivity of surface species with the $LiPF_6$-based electrolyte, storage experiments were carried out at 25 and 55°C. First, the reactivity of reference Li_2CO_3, LiOH, NiO, Li_2SO_4 and Li_2O compounds was evaluated. As its presence on NMC surface was suggested by Paulsen *et al.* [18], the reactivity of Li_2O was also investigated. Second, given the presence of significant concentration of surface species, the as-received and exposed 811 materials were tested under similar storage conditions.

3.3.1. Reactivity of reference compounds towards electrolyte

First and foremost, unlike Li_2CO_3, Li_2O, LiOH and Li_2SO_4 reference compounds, and NiO do not reveal any reactivity towards the electrolyte whatever the temperature.

Fig. 7 shows the ^{19}F NMR results of Li_2CO_3, LiOH and Li_2O at 25 and 55°C. In all cases, the doublet signal corresponding to $LiPF_6$ is centered at δ_F=-74.2 ppm (J(P,F)=709 Hz). In the case of Li_2CO_3 and Li_2O (Fig. 7 a, b and d), another doublet centered at a lower chemical shift (δ_F= -84.6 ppm, J(P,F) = 929,4 Hz) can be attributed to $LiPO_2F_2$ [43]. LiF is also clearly observed at 55°C at δ_F= -155.8 ppm (Fig. S4).

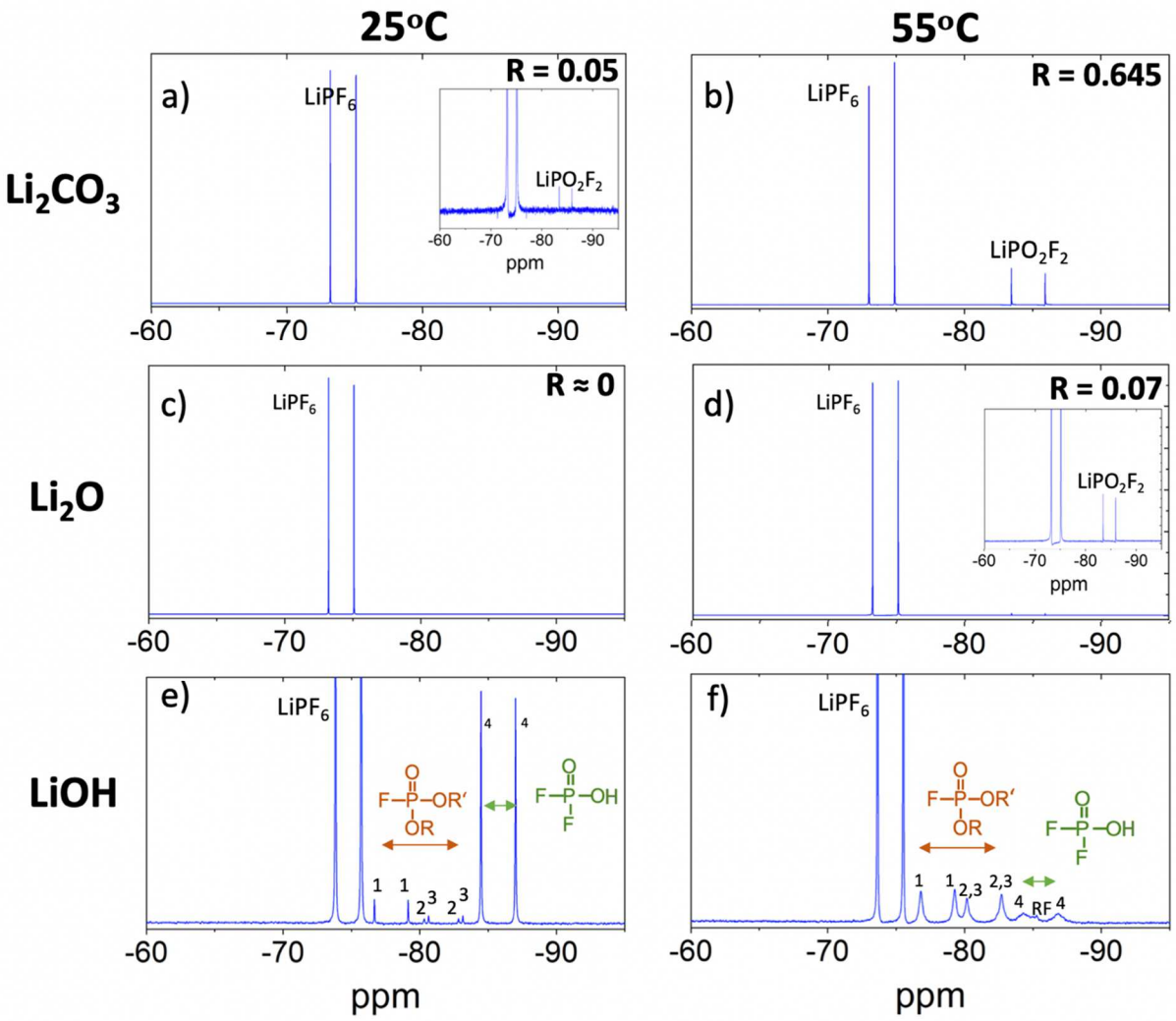

Figure 7: Liquid ^{19}F NMR spectrum of the electrolyte recovered after storage, for 4 days at 25 and 55°C, in presence of a, b) Li_2CO_3 c, d) Li_2O and e, f) LiOH with $LiPO_2F_2/LiPF_6$ molar ratio (R) as determined from peaks integration. Labels 1, 2, 3 and 4 stand for the doublets 1) $OPF(OH)_2$, 2 and 3) $OPF(OR)(OR')$ with R = CH_3 or C_2H_5 and R'= H or CH_3 or C_2H_5, and 4) $OPF_2(OH)$, respectively.

The reaction mechanism [Eqs 11 and 12] leading to $LiPO_2F_2$ can be proposed for both reactants as followed:

$$2Li_2CO_3 + LiPF_6 \rightarrow LiPO_2F_2 + 4LiF + 2CO_2 \quad [11]$$

$$2Li_2O + LiPF_6 \rightarrow LiPO_2F_2 + 4LiF \quad [12]$$

The first reaction [Eq. 11] was already proposed by Parimalam *et al.* [25] during the study of the solid electrolyte interphase (SEI) generated at the negative electrode surface. The chemical reaction of Li_2CO_3 with $LiPF_6$-based electrolyte was also investigated by Bi *et al.* [6] by making use of XRD and GC-MS techniques. They concluded that, although it was electrochemically stable, Li_2CO_3 could be chemically decomposed into LiF, and form a coating on 811 particles, along with CO_2 and POF_3 gas evolution.

The $LiPO_2F_2/LiPF_6$ molar ratios R calculated from the NMR peaks integration range from almost zero, when the reaction temperature is 25°C, to 0.645 in presence of Li_2CO_3 at 55°C. Considering the reaction stoichiometry and the starting molar ratio $M/LiPF_6$ ($M=Li_2CO_3$, Li_2O) of 1.35, a R maximum value of 2.08 can be expected. However, this value could not be reached as the $LiPO_2F_2$ solubility in carbonate solvents [44] is less than 0.5 M. On the other hand, the FTIR analysis of the white precipitate recovered after the storage test at 55°C did not reveal any Li_2CO_3 (only $LiPO_2F_2$ and $LiPF_6$). Thus, it can be concluded that the reaction [Eq. 11] is complete with Li_2CO_3 reactant at this temperature. Regarding storage test with Li_2O, the R value reaches only 0.07 at 55°C. Hence, the lithium carbonate turns out to be much more reactive towards $LiPF_6$ than Li_2O to produce $LiPO_2F_2$. This reaction generates CO_2

gas, which can have a detrimental effect on the battery lifetime. Regarding Li_2SO_4, the test at 55°C reveals the presence of a low amount of $LiPO_2F_2$ with a molar ratio R of 0.013 (Fig. S5).

Furthermore, LiOH is extremely reactive, even at 25°C. Based on previous studies [45–48], most of the peaks can be ascribed to fluorophosphates (Fig. 7 e and f) such as:

- $OPF(OH)_2$ with a doublet centered at δ_F= -77.3 ppm (J(P,F) = 927 Hz), labelled 1

- OPF(OR)(OR') with R= CH_3 or C_2H_5 and R'= H, CH_3 or C_2H_5

    - a doublet centered at δ_F= -81 ppm (J(P,F) = 944 Hz), labelled 2

    - a doublet centered at δ_F = -81.3 ppm (J(P,F) = 943 Hz), labelled 3

- $OPF_2(OH)$ with a doublet centered at δ_F= -85.2 ppm (J(P,F) = 950 Hz), labelled 4.

The temperature increase (Fig. 7f) leads to the consumption of difluorophosphate (species 4) and the formation of fluoroalcane. LiF is also clearly detected (Fig. S6), as previously in the experiments with Li_2CO_3.

As observed, the reaction with LiOH does not produce $LiPO_2F_2$, as Li_2CO_3 and Li_2O does, but on the contrary, forms fluorophosphates. The fact that lithium-based species react and lead to non-lithium-based species indicates a more complicated pathway. To account for this, we propose a two-step mechanism; i) the lithium alkyl carbonates formation by the reaction of LiOH with linear carbonates [Eq. 13]. The feasibility of this reaction was proven by FTIR analysis of reaction product after mixing EMC with LiOH at 55°C during 4 days (Fig. S7) ii) the reaction of these alkyl carbonates with $LiPF_6$ to form the fluorophosphates [Eqs 14-16] as demonstrated by Parimalam et al. [25].

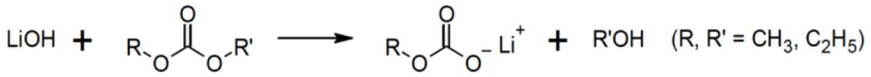

[13]

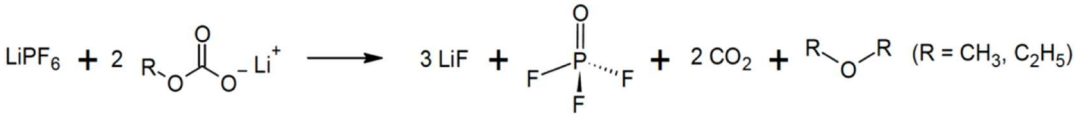

[14]

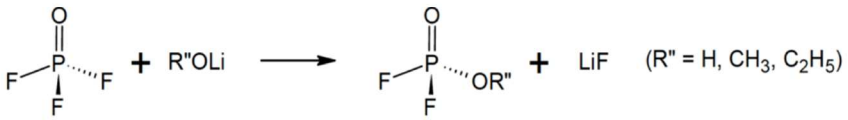

[15]

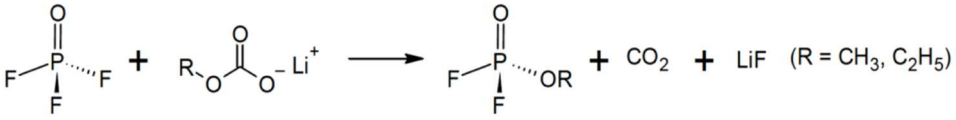

[16]

3.3.2. Reactivity of as-received and exposed 811 materials towards electrolyte

Likewise, reactivity tests were performed with the as-received and exposed 811 materials. From the ^{19}F RMN analysis, only $LiPF_6$, $LiPO_2F_2$ and LiF are detected in both materials and at both temperatures. The absence of fluorophosphates is intriguing, as they were found to be easily produced from hydroxide species. It implies that most probably, Li_2O is present at the NMC surface instead of LiOH. The lithium oxide in contact with water is transformed into LiOH by the following reaction [Eq. 17]:

$$2Li_2O + H_2O \rightarrow 2LiOH \quad [17]$$

The latter being titrated by acid-base titration. This result explains the absence of the LiOH band in FTIR spectra (Fig. S2). It is noteworthy that for the exposed 811 material, the other surface species as the oxyhydroxides or oxides, do not generate fluorophosphates when in contact with electrolyte.

The $LiPO_2F_2/LiPF_6$ molar ratios R deduced from the different NMR analyses are reported in Table 3. For both as-received and exposed materials, the $LiPO_2F_2$ formation is facilitated with

temperature increase. From these R values, the $LiPO_2F_2$ moles quantity in 1 mL of electrolyte was calculated and compared to the one expected from the complete reaction of soluble bases with electrolyte [Eqs 11 and 12], considering Li_2O and not LiOH. Note that from 25°C, for the as-received 811 material, the whole amount of soluble bases react to form $LiPO_2F_2$.

Material	SB from ABT (µmol/$g_{AM\ p.}$)		Expected $LiPO_2F_2$ from ABT results for 100 mg of NMC in 1 mL (µmol)	NMR experiments		
	Li_2CO_3	LiOH		Storage temperature (°C)	R	n $LiPO_2F_2$ in 1 mL (µmol)
811 as-received	19 ± 1	205 ± 14	6.1 ± 0.8	25	0.006	6
				55	0.007	7
811 exposed	370 ± 10	17 ± 5	18.9 ± 1.2	25	0.003	3
				55	0.013	13

Table 3. Comparison of expected $LiPO_2F_2$ from ABT results and experimental $LiPO_2F_2$ moles quantity present in 1mL of $LiPF_6$-based electrolyte after storage in presence of 100 mg of as-received and exposed NMC 811.

The highest quantity of Li_2CO_3 for the exposed NMC material leads obviously to a higher quantity of expected $LiPO_2F_2$ (18.9 *vs.* 6.1 µmol) but the transformation process seems to be slowed down as the reaction yield does not reach 100%, even at 55°C. It could be explained by the fact that the surface transformation occurring during the H_2O/CO_2 exposure leads to a complex surface layer made of oxyhydroxides, oxides and soluble bases, which makes the accessibility of $LiPF_6$ to the soluble bases more difficult.

From these experiments, we clearly demonstrated that soluble bases and Li_2SO_4 produce $LiPO_2F_2$ upon storage with $LiPF_6$-based electrolyte even at room temperature. Since it has been reported that $LiPO_2F_2$ is an efficient electrolyte additive [49], notably to decrease the impedance of the positive layered and negative electrodes, and to improve the capacity retention of batteries [50,51], it is suggested that soluble bases and Li_2SO_4 may be beneficial

to the batteries electrochemical performances. However, the surface transformation during air exposure produces other surface species as oxyhydroxides or oxides and NMC delithiation, which may affect negatively these performances.

4. Conclusion

Acid-base titration technique is relatively easy to implement and well-suited for quantifying soluble bases in NMC materials aqueous filtrates. Furthermore, it allows accurate assessment of the delithiation amount after a long-time storage or a water-washing procedure undertaken in industry for the purpose of capacity retention improvement. However, this technique revealed to be not sufficient to provide a complete characterization of the whole surface species, including water soluble and insoluble species.

This work, devoted to studying the influence of a H_2O/CO_2 atmosphere exposure onto five different NMC materials, clearly illustrated, through combined acid-base titration and TG-MS analysis, the increasing chemical instability of the materials with Ni^{3+} amount. Evidence was given that the exposition to such atmosphere brings about a chemical transformation of the surface material resulting in the lithium carbonate, nickel cobalt oxyhydroxides and nickel and manganese oxides formation following a clearly established mechanism. It was deduced that the characteristic weight loss between 150-450°C is due to the thermal decomposition of oxyhydroxides and the subsequent in-situ reaction between oxides, oxygen and lithium carbonate to reform a layered material, which may explain the partial electrochemical capacity recovery after annealing treatment of exposed NMC materials.

A stepwise investigation of the chemical reactivity of the surface species towards $LiPF_6$-based electrolyte was carried out through ^{19}F NMR measurements. As LiOH titrated through acid-base titration measurements should react with $LiPF_6$ to form fluorophosphate-type

compounds, their absence in electrolyte after contact with the pristine 811 NMC material led us to conclude that LiOH was the reaction product of Li_2O with water. The surface species, Li_2CO_3, Li_2O and Li_2SO_4 contained in the positive electrode react with $LiPF_6$ to produce $LiPO_2F_2$. The latter being known as an effective electrolyte additive, it is supposed that soluble bases and Li_2SO_4 could have a beneficial effect on capacity retention. However, the presence of insoluble bases as oxyhydroxides and oxides may increase the impedance and thus be responsible for the harmful impact of electrochemical performances storage on cells.

Acknowledgments: The financial support from the Association Nationale de la Recherche et de la Technologie (ANRT, France) is gratefully acknowledged. The authors are grateful to the UPJV microscopy platform for sharing their facilities, to Pierre-Etienne Cabelguen for the valuable comments, to Alessandra Sergent and Celia Rierny for the ICP-AES analysis, as well as to Michel Armand for fruitful discussions and advice.

REFERENCES

[1] N. Mijung, Y. Lee, J. Cho, Water Adsorption and Storage Characteristics of Optimized LiCoO2 and LiNi1／3Co1／3Mn1／3O2 Composite Cathode Material for Li-Ion Cells, J. Electrochem. Soc. 153 (2006) A935–A940. https://doi.org/10.1149/1.2186041.

[2] X. Xiong, Z. Wang, P. Yue, H. Guo, F. Wu, J. Wang, X. Li, Washing effects on electrochemical performance and storage characteristics of LiNi0.8Co0.1Mn0.1O2 as cathode material for lithium-ion batteries, Journal of Power Sources. 222 (2013) 318–325. https://doi.org/10.1016/j.jpowsour.2012.08.029.

[3] J. Park, J. Park, J. Lee, Stability of LiNi0.6Mn0.2Co0.2O2 as a Cathode Material for Lithium-Ion Batteries against Air and Moisture, Bulletin of the Korean Chemical Society. 37 (2016) 344–348. https://doi.org/10.1002/bkcs.10679.

[4] G.V. Zhuang, G. Chen, J. Shim, X. Song, P.N. Ross, T.J. Richardson, Li2CO3 in LiNi0.8Co0.15Al0.05O2 cathodes and its effects on capacity and power, Journal of Power Sources. 134 (2004) 293–297. https://doi.org/10.1016/j.jpowsour.2004.02.030.

[5] N.V. Faenza, L. Bruce, Z.W. Lebens-Higgins, I. Plitz, N. Pereira, L.F.J. Piper, G.G. Amatucci, Editors' Choice—Growth of Ambient Induced Surface Impurity Species on Layered Positive Electrode Materials and Impact on Electrochemical Performance, J. Electrochem. Soc. 164 (2017) A3727–A3741. https://doi.org/10.1149/2.0921714jes.

[6] Y. Bi, T. Wang, M. Liu, R. Du, W. Yang, Z. Liu, Z. Peng, Y. Liu, D. Wang, X. Sun, Stability of Li2CO3 in cathode of lithium ion battery and its influence on electrochemical performance, RSC Adv. 6 (2016) 19233–19237. https://doi.org/10.1039/C6RA00648E.

[7] J.M. Paulsen, H.-K. Park, Y.H. Kwon, Ni-based lithium transition metal oxide, US7648693B2, 2010.

[8] M. Bichon, D. Sotta, N. Dupré, E. De Vito, A. Boulineau, W. Porcher, B. Lestriez, Study of Immersion of LiNi0.5Mn0.3Co0.2O2 Material in Water for Aqueous Processing of Positive Electrode for Li-Ion Batteries, ACS Appl. Mater. Interfaces. 11 (2019) 18331–18341. https://doi.org/10.1021/acsami.9b00999.

[9] Z. Chen, J. Wang, J. Huang, T. Fu, G. Sun, S. Lai, R. Zhou, K. Li, J. Zhao, The high-temperature and high-humidity storage behaviors and electrochemical degradation mechanism of LiNi0.6Co0.2Mn0.2O2 cathode material for lithium ion batteries, Journal of Power Sources. 363 (2017) 168–176. https://doi.org/10.1016/j.jpowsour.2017.07.087.

[10] R. Jung, R. Morasch, P. Karayaylali, K. Phillips, F. Maglia, C. Stinner, Y. Shao-Horn, H.A. Gasteiger, Effect of Ambient Storage on the Degradation of Ni-Rich Positive Electrode Materials (NMC811) for Li-Ion Batteries, J. Electrochem. Soc. 165 (2018) A132–A141. https://doi.org/10.1149/2.0401802jes.

[11] W. Liu, G. Hu, K. Du, Z. Peng, Y. Cao, Enhanced storage property of LiNi0.8Co0.15Al0.05O2 coated with LiCoO2, Journal of Power Sources. 230 (2013) 201–206. https://doi.org/10.1016/j.jpowsour.2012.12.065.

[12] X. Zhang, W.J. Jiang, X.P. Zhu, A. Mauger, Qilu, C.M. Julien, Aging of LiNi1/3Mn1/3Co1/3O2 cathode material upon exposure to H2O, Journal of Power Sources. 196 (2011) 5102–5108. https://doi.org/10.1016/j.jpowsour.2011.02.009.

[13] I.A. Shkrob, J.A. Gilbert, P.J. Phillips, R. Klie, R.T. Haasch, J. Bareño, D.P. Abraham, Chemical Weathering of Layered Ni-Rich Oxide Electrode Materials: Evidence for Cation Exchange, J. Electrochem. Soc. 164 (2017) A1489–A1498. https://doi.org/10.1149/2.0861707jes.

[14] H.S. Liu, Z.R. Zhang, Z.L. Gong, Y. Yang, Origin of Deterioration for LiNiO2 Cathode Material during Storage in Air, Electrochem. Solid-State Lett. 7 (2004) A190–A193. https://doi.org/10.1149/1.1738471.

[15] K. Matsumoto, R. Kuzuo, K. Takeya, A. Yamanaka, Effects of CO2 in air on Li deintercalation from LiNi1−x−yCoxAlyO2, Journal of Power Sources. 81–82 (1999) 558–561. https://doi.org/10.1016/S0378-7753(99)00216-5.

[16] K. Shizuka, C. Kiyohara, K. Shima, Y. Takeda, Effect of CO2 on layered Li1+zNi1−x−yCoxMyO2 (M=Al, Mn) cathode materials for lithium ion batteries, Journal of Power Sources. 166 (2007) 233–238. https://doi.org/10.1016/j.jpowsour.2007.01.013.
[17] J. Paulsen, J. Kim, High nickel cathode material having low soluble base content, US9698418B2, 2017.
[18] J.M. Paulsen, H.-K. Park, Y.H. Kwon, Process of making cathode material containing Ni-based lithium transition metal oxide, US7943111B2, 2011. https://patents.google.com/patent/US7943111B2/en (accessed December 9, 2019).
[19] K. Matsumoto, R. Kuzuo, K. Takeya, A. Yamanaka, Effects of CO2 in air on Li deintercalation from LiNi1yxyyCo x Al yO2, (1999) 4.
[20] H. Liu, Y. Yang, J. Zhang, Investigation and improvement on the storage property of LiNi0.8Co0.2O2 as a cathode material for lithium-ion batteries, Journal of Power Sources. 162 (2006) 644–650. https://doi.org/10.1016/j.jpowsour.2006.07.028.
[21] A Dictionary of Chemistry, 6th ed., in: J. Daintith, Oxford University Press, 2008: p. 330.
[22] J. Sicklinger, M. Metzger, H. Beyer, D. Pritzl, H.A. Gasteiger, Ambient Storage Derived Surface Contamination of NCM811 and NCM111: Performance Implications and Mitigation Strategies, J. Electrochem. Soc. 166 (2019) A2322–A2335. https://doi.org/10.1149/2.0011912jes.
[23] Smith O.C., Identification and Qualitative Chemical Analysis of Minerals, second edition, D. Van Nostrand, Princeton, N.J., 1953.
[24] I.A. Shkrob, J.A. Gilbert, P.J. Phillips, R. Klie, R.T. Haasch, J. Bareño, D.P. Abraham, Chemical Weathering of Layered Ni-Rich Oxide Electrode Materials: Evidence for Cation Exchange, J. Electrochem. Soc. 164 (2017) A1489–A1498. https://doi.org/10.1149/2.0861707jes.
[25] B.S. Parimalam, A.D. MacIntosh, R. Kadam, B.L. Lucht, Decomposition Reactions of Anode Solid Electrolyte Interphase (SEI) Components with $LiPF_6$, The Journal of Physical Chemistry C. 121 (2017) 22733–22738. https://doi.org/10.1021/acs.jpcc.7b08433.
[26] D. Aurbach, K. Gamolsky, B. Markovsky, G. Salitra, Y. Gofer, U. Heider, R. Oesten, M. Schmidt, The Study of Surface Phenomena Related to Electrochemical Lithium Intercalation into Li x MO y Host Materials (M = Ni, Mn), J. Electrochem. Soc. 147 (2000) 1322–1331. https://doi.org/10.1149/1.1393357.
[27] A.A. Benedetti-Pichler, M. Cefola, Warder's method for the titration of carbonates, Industrial & Engineering Chemistry Analytical Edition. 11 (1939) 327–332. https://doi.org/10.1021/ac50134a012.
[28] Warder, R.B., Chem. News. 43 (1881) 228.
[29] H.-J. Noh, S. Youn, C.S. Yoon, Y.-K. Sun, Comparison of the structural and electrochemical properties of layered Li[NixCoyMnz]O2 (x = 1/3, 0.5, 0.6, 0.7, 0.8 and 0.85) cathode material for lithium-ion batteries, Journal of Power Sources. 233 (2013) 121–130. https://doi.org/10.1016/j.jpowsour.2013.01.063.
[30] D. Pritzl, T. Teufl, A.T.S. Freiberg, B. Strehle, J. Sicklinger, H. Sommer, P. Hartmann, H.A. Gasteiger, Editors' Choice—Washing of Nickel-Rich Cathode Materials for Lithium-Ion Batteries: Towards a Mechanistic Understanding, Journal of The Electrochemical Society. 166 (2019) A4056–A4066. https://doi.org/10.1149/2.1351915jes.
[31] R. Moshtev, P. Zlatilova, S. Vasilev, I. Bakalova, A. Kozawa, Synthesis, XRD characterization and electrochemical performance of overlithiated LiNiO2, Journal of Power Sources. 81–82 (1999) 434–441. https://doi.org/10.1016/S0378-7753(99)00247-5.
[32] X. Xiong, Z. Wang, P. Yue, H. Guo, F. Wu, J. Wang, X. Li, Washing effects on electrochemical performance and storage characteristics of LiNi0.8Co0.1Mn0.1O2 as cathode material for lithium-ion batteries, Journal of Power Sources. 222 (2013) 318–325. https://doi.org/10.1016/j.jpowsour.2012.08.029.
[33] D.D. Williams, R.R. Miller, Effect of Water Vapor on the $LiOH\text{-}CO_2$ Reaction. Dynamic Isothermal System, Ind. Eng. Chem. Fund. 9 (1970) 454–457. https://doi.org/10.1021/i160035a024.

[34] J. Sicklinger, M. Metzger, H. Beyer, D. Pritzl, H.A. Gasteiger, Ambient Storage Derived Surface Contamination of NCM811 and NCM111: Performance Implications and Mitigation Strategies, J. Electrochem. Soc. 166 (2019) A2322–A2335. https://doi.org/10.1149/2.0011912jes.
[35] K. Shizuka, C. Kiyohara, K. Shima, K. Okahara, K. Okamoto, Y. Takeda, Effect of CO2 on Layered Li1+zNi1-x-yCoxMyO2 (M=Al,Mn) Cathode Materials, in: ECS Transactions, ECS, Washington, DC, 2008: pp. 7–13. https://doi.org/10.1149/1.2938901.
[36] D.R. Biswas, Thermal energy storage using sodium sulfate decahydrate and water, Solar Energy. 19 (1977) 99–100. https://doi.org/10.1016/0038-092X(77)90094-9.
[37] N. Koga, H. Tanaka, Kinetics and mechanisms of the thermal dehydration of dilithium sulfate monohydrate, The Journal of Physical Chemistry. 93 (1989) 7793–7798. https://doi.org/10.1021/j100360a014.
[38] M. Komath, S. Thomas, K.A. Cherian, A. Ray, Preparation of gamma-nickel oxyhydroxide through high temperature reaction of nickel with anhydrous sodium hydroxide, Materials Chemistry and Physics. 36 (1993) 190–193. https://doi.org/10.1016/0254-0584(93)90032-H.
[39] J. Pan, Y. Sun, P. Wan, Z. Wang, X. Liu, Synthesis, characterization and electrochemical performance of battery grade NiOOH, Electrochemistry Communications. 7 (2005) 857–862. https://doi.org/10.1016/j.elecom.2005.05.004.
[40] F. Bardé, M.R. Palacín, B. Beaudoin, J.-M. Tarascon, Ozonation: A Unique Route To Prepare Nickel Oxyhydroxides. Synthesis Optimization and Reaction Mechanism Study, Chem. Mater. 17 (2005) 470–476. https://doi.org/10.1021/cm040133+.
[41] J.H. Jo, C.-H. Jo, H. Yashiro, S.-J. Kim, S.-T. Myung, Re-heating effect of Ni-rich cathode material on structure and electrochemical properties, Journal of Power Sources. 313 (2016) 1–8. https://doi.org/10.1016/j.jpowsour.2016.02.015.
[42] S. Jeong, J. Kim, J. Mun, Self-Generated Coating of $LiCoO_2$ by Washing and Heat Treatment without Coating Precursors, Journal of The Electrochemical Society. 166 (2019) A5038–A5044. https://doi.org/10.1149/2.0071903jes.
[43] K. Tasaki, K. Kanda, S. Nakamura, M. Ue, Decomposition of LiPF6 and Stability of PF5 in Li-Ion Battery Electrolytes. Density Functional Theory and Molecular Dynamics Studies., ChemInform. 35 (2004). https://doi.org/10.1002/chin.200407001.
[44] P. Garcia-Juan, A. Schulz, Manufacture of Mixtures Comprising Lipo2f2 and Lipf6, WO/2013/023902, 2013. https://patentscope.wipo.int/search/en/detail.jsf?docId=WO2013023902 (accessed January 8, 2020).
[45] C.L. Campion, W. Li, B.L. Lucht, Thermal Decomposition of LiPF6-Based Electrolytes for Lithium-Ion Batteries, J. Electrochem. Soc. 152 (2005) A2327–A2334. https://doi.org/10.1149/1.2083267.
[46] A.V. Plakhotnyk, L. Ernst, R. Schmutzler, Hydrolysis in the system LiPF6—propylene carbonate—dimethyl carbonate—H2O, Journal of Fluorine Chemistry. 126 (2005) 27–31. https://doi.org/10.1016/j.jfluchem.2004.09.027.
[47] B. Ravdel, K.M. Abraham, R. Gitzendanner, J. DiCarlo, B. Lucht, C. Campion, Thermal stability of lithium-ion battery electrolytes, Journal of Power Sources. 119–121 (2003) 805–810. https://doi.org/10.1016/S0378-7753(03)00257-X.
[48] S. Wilken, M. Treskow, J. Scheers, P. Johansson, P. Jacobsson, Initial stages of thermal decomposition of LiPF6-based lithium ion battery electrolytes by detailed Raman and NMR spectroscopy, RSC Adv. 3 (2013) 16359–16364. https://doi.org/10.1039/C3RA42611D.
[49] G. Yang, J. Shi, C. Shen, S. Wang, L. Xia, H. Hu, H. Luo, Y. Xia, Z. Liu, Improving the cyclability performance of lithium-ion batteries by introducing lithium difluorophosphate ($LiPO_2F_2$) additive, RSC Advances. 7 (2017) 26052–26059. https://doi.org/10.1039/C7RA03926C.
[50] C. Wang, L. Yu, W. Fan, R. Liu, J. Liu, L. Ouyang, L. Yang, M. Zhu, Enhanced high-voltage cyclability of LiNi0.5Co0.2Mn0.3O2-based pouch cells via lithium difluorophosphate introducing as electrolyte additive, Journal of Alloys and Compounds. 755 (2018) 1–9. https://doi.org/10.1016/j.jallcom.2018.05.005.

[51] Q. Lei, T. Yang, X. Zhao, W. Fan, W. Wang, L. Yu, S. Guo, X. Zuo, R. Zeng, J. Nan, Lithium difluorophosphate as a multi-functional electrolyte additive for 4.4V LiNi0.5Co0.2Mn0.3O2/graphite lithium ion batteries, Journal of Electroanalytical Chemistry. 846 (2019) 113141. https://doi.org/10.1016/j.jelechem.2019.05.023.